Circular accelerators with effective dc induction acceleration

Ken Takayama,[1] Jun Hasegawa,[2] Toshikazu Adachi,[1] Katsuya Okamura,[1] Kazumi Egawa,[1] Toshiaki Tauchi,[1] and Takashi Yoshimoto[1]

[1]*High Energy Accelerator Research Organization (KEK), Accelerator Laboratory, Oho 1-1, Tsukuba Ibaraki, 305 Japan*
[2]*Institute of Science Tokyo, Laboratory for Zero-Carbon Energy, Ookayama 2-12-1, Meguro Tokyo, 152 Japan*

(Received 3 October 2025; accepted 3 March 2026; published 7 April 2026)

Technical details of a recently proposed system for direct current (dc) induction acceleration are described. This dc induction acceleration system comprises two induction cells, each with two insulating gaps; one acts as an acceleration gap, and the other is placed on the outer cage of the induction cell to act as a resetting gap. Both gaps are bridged by diodes. The system is energized by a bipolar switching power supply. Continuous dc acceleration is limited by the saturation of magnetic materials distributed along the beam line, such as the beam-guiding magnets that act as effective absorbers of the magnetic flux that is released into the surrounding area upon resetting of the induction acceleration cell core. A secondary loop current (the primary loop current being the current that excites the magnetic core of the induction acceleration cell) necessarily flows on the metal beam-chamber surface distributed along the accelerator ring. This secondary loop current tends to degrade the resetting of the induction acceleration core and must be canceled by an artificially added tertiary loop current, whose loop passes symmetrically through the guiding magnets but bypasses the dc induction acceleration cells. In this way, resetting of the induction cores is secured at the expense of magnet saturation. dc induction acceleration can be performed via intermittent operation to release the absorbed extra flux. The effects of this externally absorbed flux on the beam orbit and optics are discussed. Applications of the dc induction acceleration are of practical interest. In addition, proposals are made for a dc induction microtron and a fixed field alternating gradient accelerator for heavy ions, which could replace existing electrostatic accelerators such as Van de Graaff or tandem accelerators, and an isochronous storage ring with dc induction acceleration for electrons/positrons, which could lead to the ultimate form in efficient continuous wave free-electron laser.

DOI: 10.1103/r4w4-qypt

I. INTRODUCTION

Takayama [1,2] proposed a novel method for accelerating a direct current (dc) beam in a circular ring. The key feature is the use of a pair of induction acceleration cells with multiple-insulating gaps. Both cells are energized by a single bipolar pulse modulator. Each cell has two insulating gaps: one is for beam acceleration, and the other, which is placed on the outer case of the induction cell, is for resetting the induction core material. In Sec. II, the operating principles and devices are reviewed for the most promising scheme. Here, the setting and resetting current is defined as the primary loop current I_1.

Since the original proposal [1], our research team has critically examined various aspects of accelerators employing the dc induction acceleration cells. In particular, it has been found that the secondary loop current, I_2, that is induced on the metal beam chamber, being associated with resetting of the magnetic cores, plays a crucial role in setting the practical limits of continuous dc acceleration. I_2, which accumulates as a result of repeated setting/resetting of the two cells, tends to substantially reduce core resetting, resulting in imperfect resetting of the induction cores. Also, I_2 perturbs the guiding magnetic fields. In Sec. III A, the effects of I_2 are analyzed for their importance and then estimated quantitatively, assuming a typical circular ring accelerator.

The temporal evolution of I_2 depends on the circuit elements placed along the secondary loop such as the inductances and resistances of the beam chamber and all the guiding magnets, which are coupled through I_2. Possible methods for reducing I_2 have been studied, and an effective way to guarantee complete induction core resetting is to add a tertiary current (I_3) loop that bypasses the pair of induction cells and is driven by a compensating power supply with a compensation voltage $V_c(t)$ chosen to

yield $I_2 = 0$. Here, I_3 is not zero and increases with continuous setting/resetting of the induction cells; this I_3 is regarded as a one-turn-coil current to the guiding magnets. If the guiding magnets are excited long before reaching saturation, then the magnets themselves should work as a type of magnetic flux storage (MFS), to which the magnetic flux originating from the reset core is transferred. In this case, however, perturbations in the guiding magnetic fields may remain. Their magnitudes are examined for typical bending and focusing magnets. If these perturbations are intolerable, an additional axisymmetric MFS centered on the beam chamber is required. The MFS is energized by the compensation voltage power supply through the tertiary current loop so as to yield $I_2 = 0$. There is no magnetic field perturbation because the tertiary current loop is isolated from the guiding magnets. Details are given in Sec. IV.

In both MFS cases (the guiding magnets themselves and external inductance), MFS saturation imposes constraints on the continuous operation of dc induction acceleration. Once saturated, the guiding magnets or external MFS must be reset, and dc induction acceleration must inevitably be stopped. If the application is in an electron storage ring, then the stored dc beam may be refreshed. In other applications, dc induction acceleration will be operated in intervals with short breaks, during which the MFS is reset.

To date, the induction synchrotron has been developed extensively at KEK [3,4], where barrier bucket induction acceleration is used. Also, the induction FFAG (fixed field alternating gradient) accelerator has been proposed [5], and the feasibility of the induction microtron has been studied [6,7]. All previous hadron induction accelerators have been based on pulse induction acceleration, but an attractive idea is to introduce the present dc induction acceleration into fixed field accelerators of the microtron and FFAG type. dc FFAG and microtron accelerators would then become substitutes for electrostatic accelerators such as Cockroft—Walton and Van de Graaf accelerators, and a particular standout would be high-energy machines beyond 10 MeV, for which there are no competitors. The former may be a promising dc accelerator for neutral beam injection to the DEMO fusion reactors, which require D^- beams of 1.5 MeV, 30 A, and a pulse duration of 3600 s. As proposed in Ref. [2], the electron storage ring capable of accommodating a dc electron beam is unique. An isochronous storage ring such as NewSUBARU [8,9], with dc induction acceleration provides the possibility of a continuous-wave (cw) free-electron laser, where FEL microbunches can circulate in the ring without decay of the bunch structure, enjoying a notably high gain. If the extreme ultraviolet (EUV) FEL with an output power of a kW level and a high efficiency of 20% is demonstrated, it should be a kind of breakthrough in the EUV lithography field. Essential features of these accelerators will be described in Sec. VI.

dc beam induction acceleration itself may be compared with repeated acceleration realized with a long induction pulse voltage in the classical FFAG. Discussion of similarities or differences is given in Appendix B.

II. PRINCIPLE OF DC INDUCTION ACCELERATION AND KEY DEVICE

The principal idea has been discussed [2], where the second insulating gap for resetting the induction magnetic core was introduced and the flip-flop opening/closing of the two insulating gaps was proposed. The original proposal assumed either an active (i.e., SiC-MOSFET) or passive (i.e., diode) switching device for closing/opening of the insulating gaps; herein, discussion is limited to the use of diodes. The dc induction acceleration system comprises a single pair of cells A and B, each with two insulating gaps and that are driven by a common current I_1 from a bipolar switching power supply. When the bipolar switching power supply is turned on, the current flows through the induction acceleration circuit as shown in Fig. 1. Cell A is set when

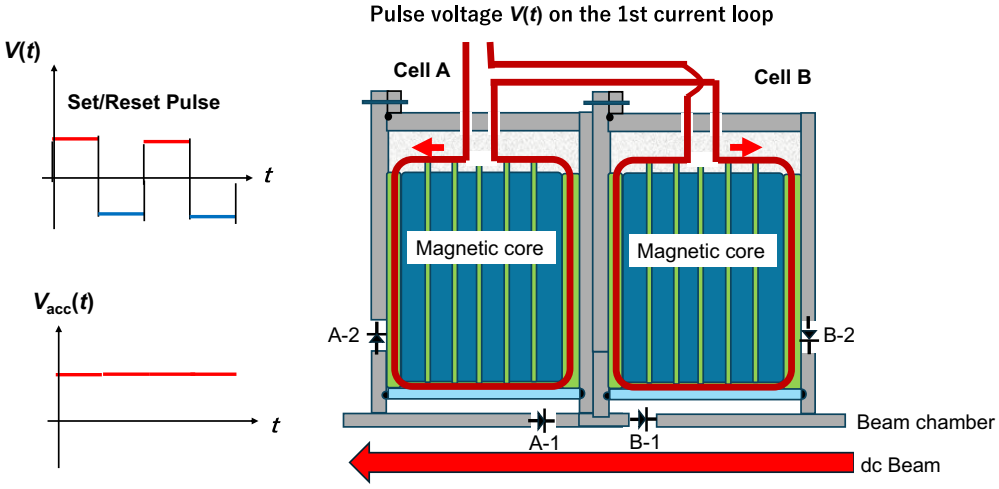

FIG. 1. Schematic view of the dc induction acceleration unit.

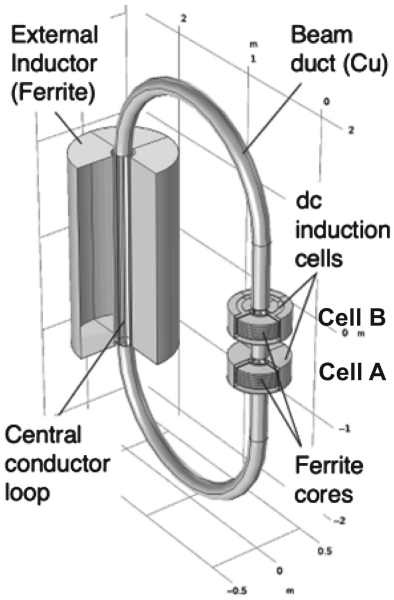

FIG. 2. COMSOL simulation model for dc induction acceleration in a circular ring, where the external inductor represents the guiding magnets or the real external inductance as a flux absorber. Assumed circuit parameters: cell inductance of 110 μH, resistance of 330 Ω, and flux storage inductance of 110 mH.

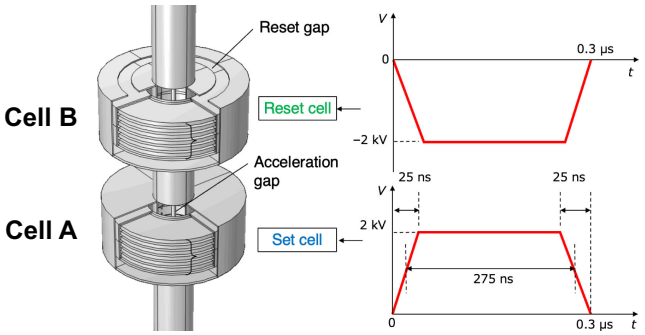

FIG. 3. Added pulse voltage profiles in the set-reset model.

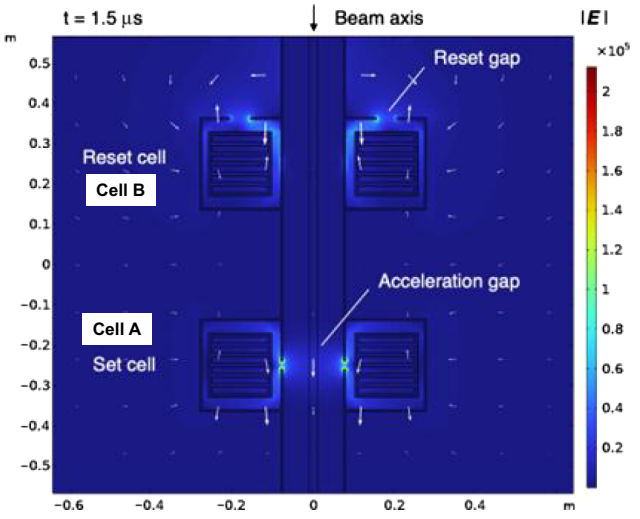

FIG. 4. Electric fields in the set-reset model.

diode Ad-1 opens and diode Ad-2 simultaneously closes; the acceleration voltage is generated across gap A-1. Simultaneously, Bd-1 closes and Bd-2 opens, whereupon the magnetic core of cell B is demagnetized. This process is repeated in a flip-flop mode, resulting in a flat voltage through the dc induction acceleration module. This is the operating principle.

Although there are still questions about whether the diodes can work as expected and withstand the radiation in an accelerator tunnel, the principle itself is very simple. Therefore, to determine whether the present dc induction acceleration system can really work in circular rings, we must investigate the present dc induction acceleration carefully in a full-scale accelerator, because the magnetic flux in cell B exits through gap B-2 when cell B is reset. The metal beam chamber will work as a secondary current loop for cell B itself, where the primary loop is the reset current loop of cell B, as mentioned in Sec. I. Using Faraday's law, it is easily predicted that the secondary loop current I_2 is induced on the metal chamber connected with the outer metal cage of cell A.

To confirm this primitive prediction, COMSOL simulations [10] have been carried out, assuming an appropriate configuration as shown in Fig. 2. Here, the copper beam duct is isolated from the ground, and the external inductor represents either an integration of bending magnets, quadrupole magnets, and correction magnets in most cases or the actual external inductor as MFS apart from the guiding magnets. For simplicity, two induction cells are excited independently by voltage pulse profiles shown in Fig. 3. All the diodes shown in Fig. 1 are assumed to function ideally are simulated by four conductor rods with a diameter of 1 cm. Figure 4 shows the generated electric field distribution. As can be seen, the acceleration field is localized near the acceleration gap and is unaffected by the resetting of the reset cell, as predicted.

Induced on the beam chamber, current I_2 should be reduced remarkably by the existence of the external inductor but gradually increase as a result of the repeated resetting of cells A and B. However, this is unclear in the above COMSOL simulation for just a single shot. Note that the secondary loop current I_2 can ruin the resetting of cells A and B over a long period of time.

In Sec. III, issues associated with I_2 are discussed and intrinsic countermeasures against them are described.

III. ISSUES ASSOCIATED WITH SECONDARY LOOP CURRENT INDUCED ON THE BEAM CHAMBER

A. Imperfect resetting

In the process of setting cell A and resetting cell B, the beam chamber topologically surrounds the magnetic core

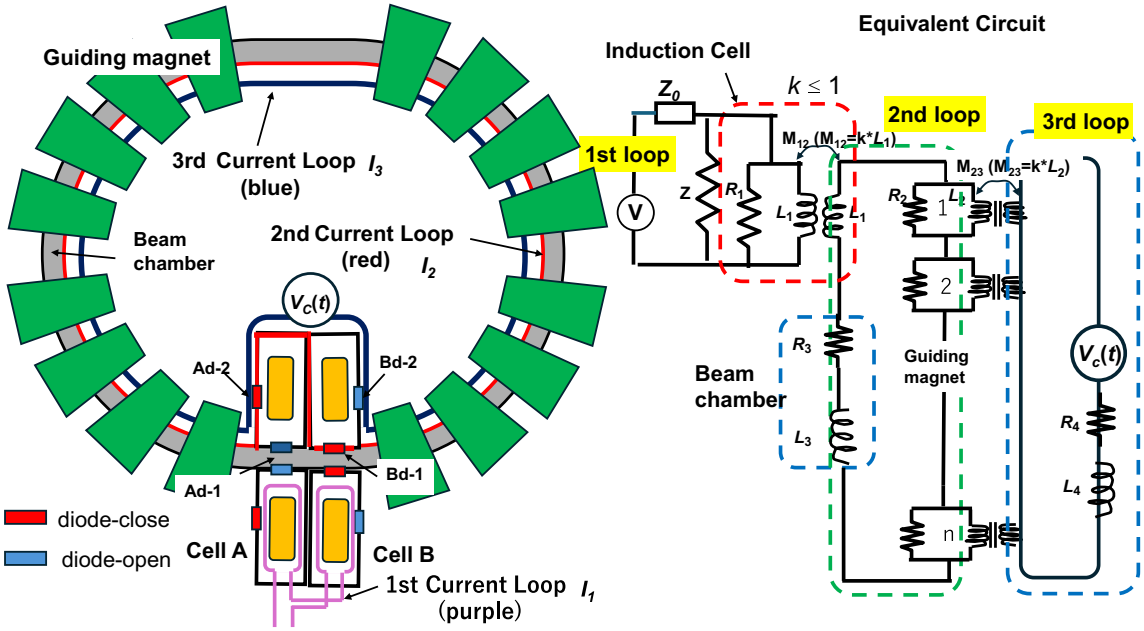

FIG. 5. Schematic view of a circular ring with dc induction acceleration with the compensation current loop and the equivalent circuit including the entire accelerator system.

in cell B along the path through the closing diode Bd-1, the outer case of cell A, and the closing diode Ad-2. In the opposite process, it surrounds the magnetic core in cell A along the path through the closing diode Ad-1, the outer case of cell B, and the closing diode Bd-2 (see the left-hand side of Fig. 5, especially the secondary current loop shown by the red line). Thus, I_2 increases continuously in magnitude during continuous operation in the absence of the beam-guiding magnets in the secondary loop and the compensation circuit shown in Fig. 5. Thus, this increasing I_2 inevitably blocks the resetting process of cells A and B, and so continuous dc acceleration is impossible in this state.

However, the reality is that the magnitude of I_2 in the early stage of dc acceleration is affected strongly by the huge inductance of the guiding magnets placed along the beam chamber. Our theoretical calculations based on a typical 1-GeV electron storage ring with a circumference of 100 m for a synchrotron radiation source have shown that I_2 reaches several tens of amperes after 1 ms of dc operation. From the perspective of resetting the magnetic core, this magnitude is still large and cannot be tolerated.

B. Perturbation of guiding magnetic fields

The secondary loop current must be regarded as a one-turn coil for the guiding magnets. Note that this current flows uniformly on the beam chamber in one direction. If the geometrical structure of the guiding magnet core is axially symmetric, then perturbation of the guiding magnetic fields should be limited. In Sec. IV, the magnitude of this perturbation is estimated.

IV. COMPENSATION OF THE SECONDARY CURRENT EFFECTS

As argued in Sec. III, I_2 inevitably inhibits complete resetting of the induction acceleration core. Therefore, from the circuit theory, we have the natural idea of introducing the tertiary loop to reduce I_2. Concern about imperfect resetting is resolved if $I_2 = 0$. The required tertiary current loop can be achieved in one of two ways: either as already shown in Fig. 5, or as shown in Fig. 10 in Sec. IV B.

A. Guiding magnets as a magnetic flux storage

Although the tertiary current loop passes through all of the guiding magnets in parallel with the beam chamber, it bypasses the induction cell, as seen in Fig. 5. The tertiary current loop is driven by the compensation power supply $V_c(t)$, which is operated so as to fully cancel I_2. Consequently, resetting of the magnetic cores in the induction cells is secured. Note here that I_3 still flows on the external current loop along the beam chamber through the guiding magnets, as shown by the blue line in Fig. 5. Details of circuit analysis where the compensation circuit loop is assumed is given in Appendix A. The compensation voltage $V_c(t)$ that gives $I_2 = 0$ is evaluated by solving simultaneous differential equations that stand for each circuit loop. The currents in the first loop and inertial loop are schematically depicted in Figs. 15–17.

The field perturbations due to the tertiary current still remain, but their size is easily estimated, if we assume a typical window-frame bending magnet and quadrupole magnet. Our field calculations show that the effects are negligibly small, as seen in Figs. 6–9 and so continuous dc

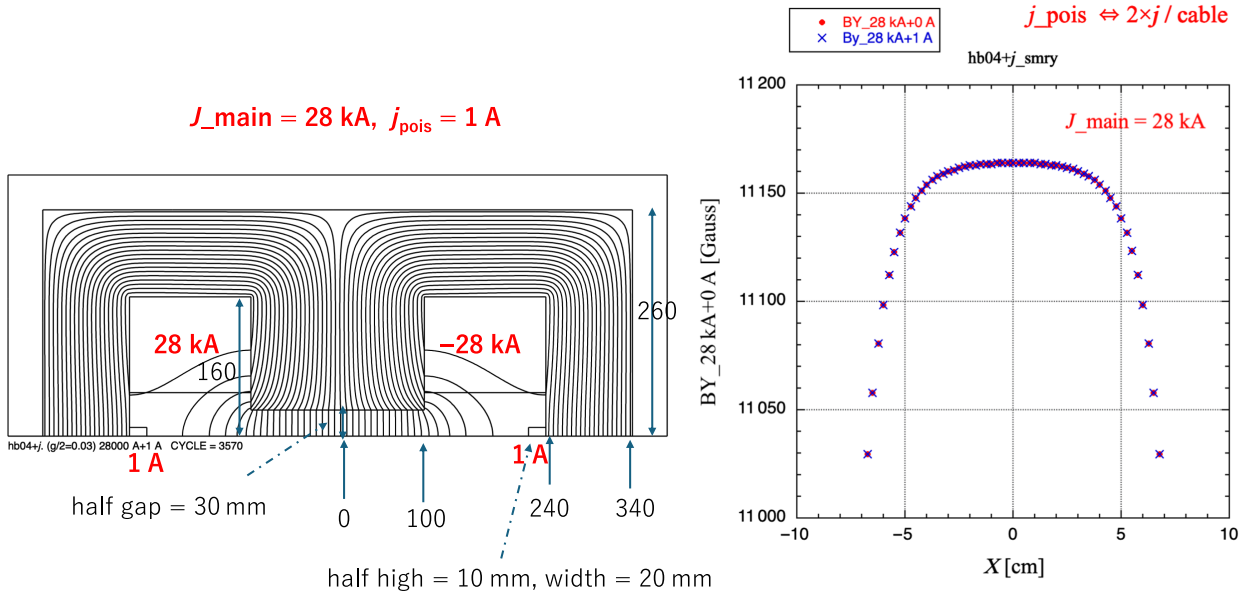

FIG. 6. Dipole fields with the compensation current I_3, where the dipole fields of about 1.1 T is excited by the dipole current of 28 kA and I_3 of 2 A flowing with the symmetry to the magnetic core is assumed.

acceleration should be possible, until the guiding magnets reach saturation. As long as I_3 flows in magnet regions symmetrically arranged with respect to the magnetic core, the field errors are not observable. The tertiary current loop is divided into two lines for the dipole magnets and four lines for the quadrupole magnets.

B. External magnetic flux storage

It is possible for the tertiary current loop to couple with the secondary current loop through the external MFS without directly affecting the guiding magnets and the induction magnetic core. Figure 10 shows this both schematically and topologically. The axisymmetric MFS is placed on the beam line. The tertiary current loop is driven by the external power supply $V_c(t)$ so as to cancel I_2 in a way similar to that in Sec. IV A. The induced fields in the MFS by I_3 never affect the beam orbit or beam profile in the transverse direction because of its axis symmetry, as long as the MFS is kept before its magnetic material reaches saturation.

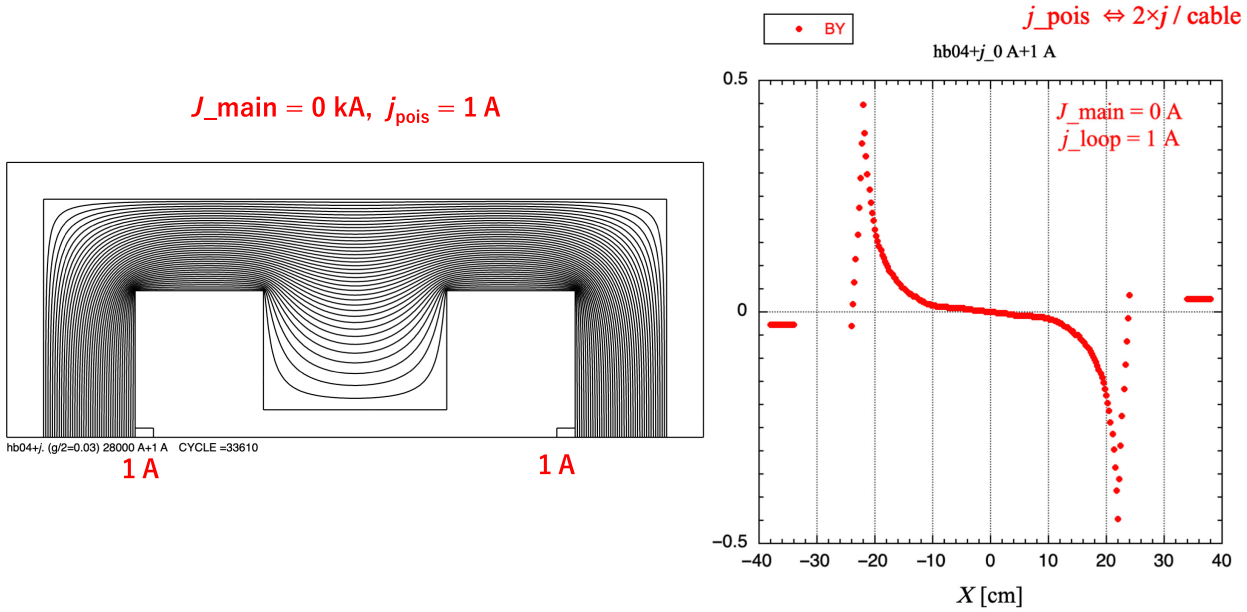

FIG. 7. Magnetic flux induced by I_3 of 2 A. Flux lines are confined inside the magnetic core.

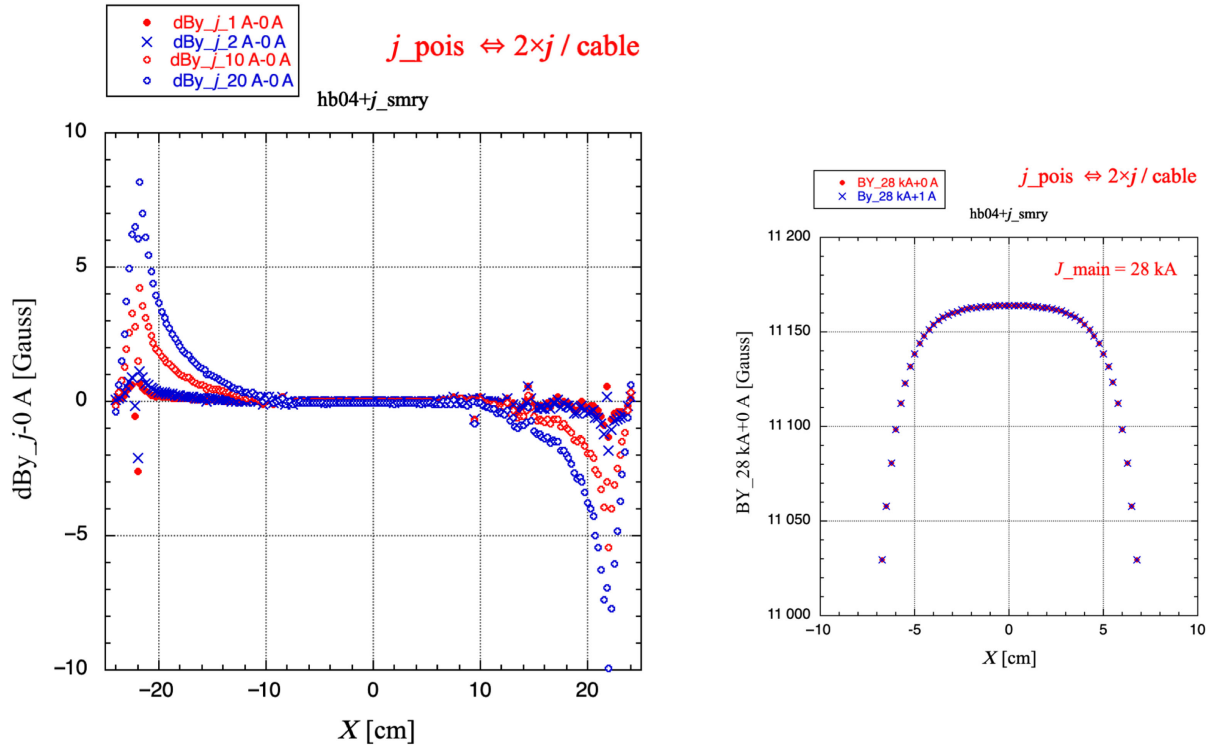

FIG. 8. Magnetic flux deviation as a function of I_3 There are no notable field errors even for I_3 of 40 A.

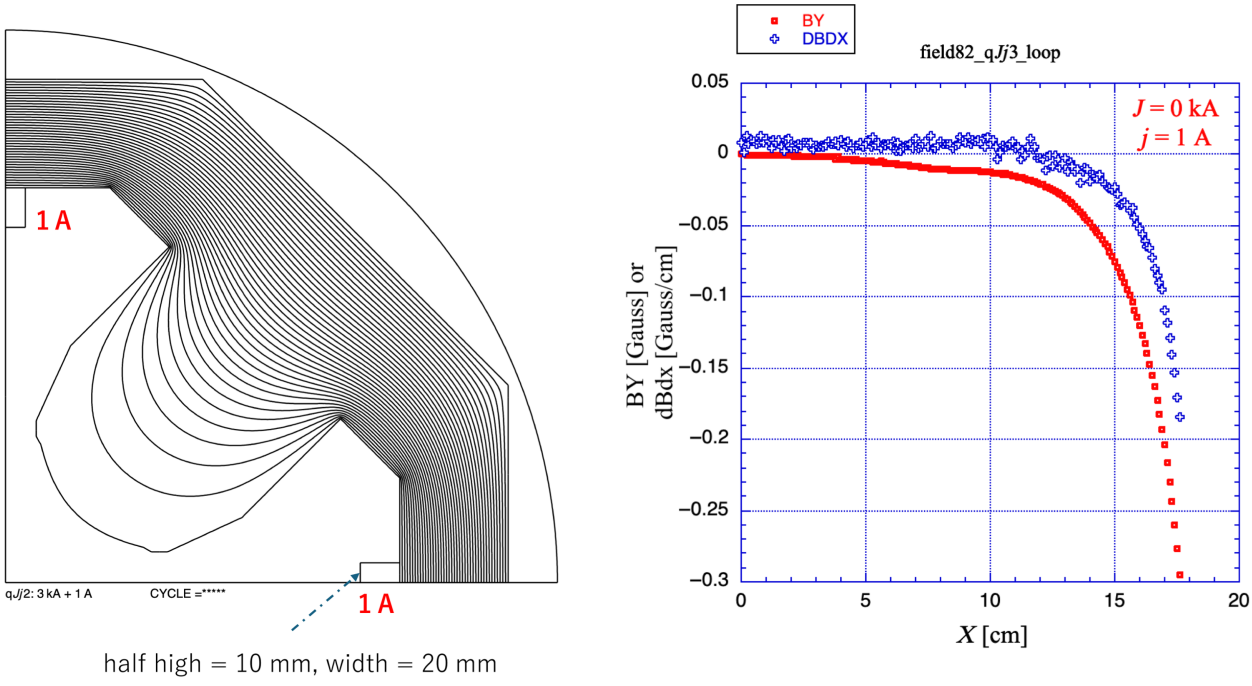

FIG. 9. Magnetic flux in a typical quadrupole magnet core and the flux density and field gradient on the median plane for $I_3 = 4$ A.

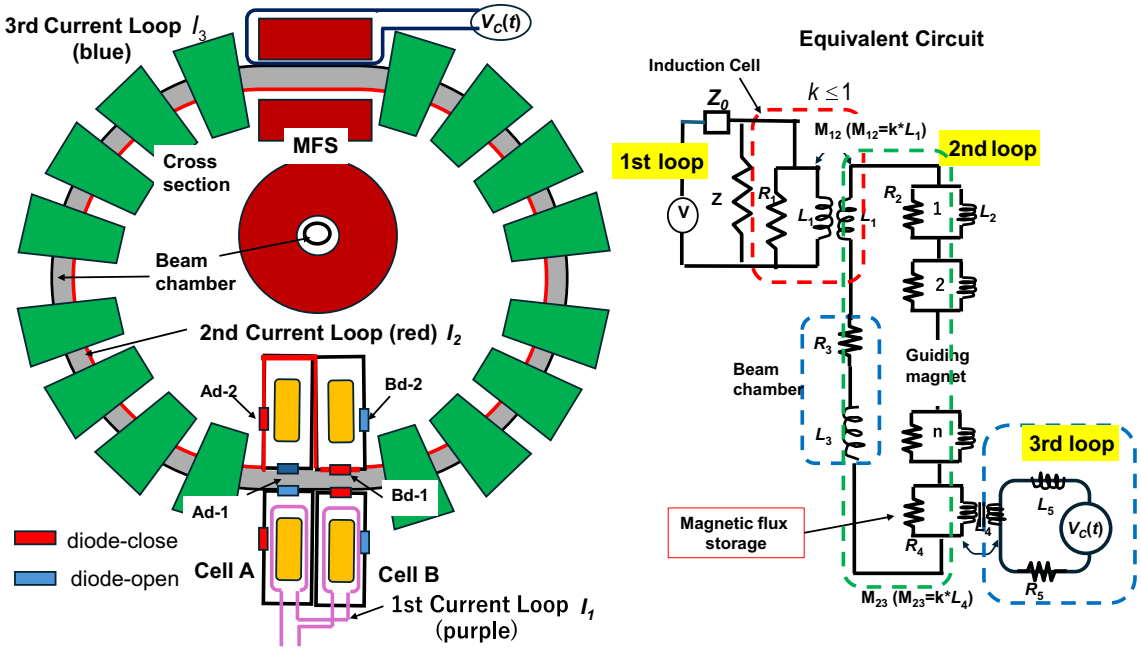

FIG. 10. A compensation circuit with the external magnetic flux storage and its equivalent circuit.

V. LIMIT ON CONTINUOUS DC ACCELERATION

As discussed in Sec. IV, continuous dc acceleration is feasible as long as the magnetic flux from the induction acceleration cells can be transferred into the guiding magnets or external MFS with the help of I_3 or the compensation power supply. The maximum time duration of continuous dc operation depends simply on the acceptable magnetic flux in the guiding magnets or external MFS of the accelerator. Either way, a linear increase in I_3 of a few tenths of an ampere seems to be accepted. In most cases, the expectation is for continuous dc operation on the order of milliseconds, and this corresponds to 3000 turns in an electron storage ring with the circumference of 100 m.

During the time needed to reset the extra flux in the guiding magnets and the MFS originating from the induction cores, which ranges from microseconds to milliseconds, dc beam injection is stopped, or the dc beam must be refreshed if the accelerator with dc acceleration is a storage ring.

VI. TYPICAL EXAMPLES OF ACCELERATORS WITH DC ACCELERATION

The dc ion accelerators introduced in this section are attractive as high-energy ion drivers, the energy and beam intensity of which far exceed those of Van de Graaff accelerator or tandem accelerators. Furthermore, these dc ion accelerators would meet the demands of future magnetic fusion beyond ITER (e.g., a 1.5- to 3-MeV D^- beam for neutral beam injection in DEMO fusion reactor [11]). dc electron accelerators can also open up new fields for cw FELs in electron storage rings; here, the microbunch structure with the FEL resonance frequency can be accommodated, and the energy losses due to FEL interaction and synchrotron radiation are compensated by dc induction acceleration.

These dc accelerators are characterized by high intensity and high efficiency. Properties originate simply from the characteristics of a "dc beam with induction acceleration." The high-intensity comes from the low space-charge effects in the transverse direction; meanwhile, those in the longitudinal direction disappear completely. The induction acceleration device is low impedance in nature. As a result, beam loading does not become a big issue, unlike rf acceleration [3]. The main losses of the induction acceleration system are the switching losses in the SiC-MOSFETs [12] and the magnetic core loss [13], with an estimated overall efficiency of around 63%. In addition, wakefields in accelerator components are not a problem, because the beam has no bunch structure coupling with the beam environment.

A. dc induction cell unit

Here, a typical example of the dc induction cell unit is given. Its parameters are extrapolated from those of the existing 50% duty (or pulse mode) induction cell for the induction synchrotron developed at KEK [3]. From Faraday's law, the induced voltage V with a pulse width of τ across the acceleration gaps A-1 or B-1 in Fig. 1 is

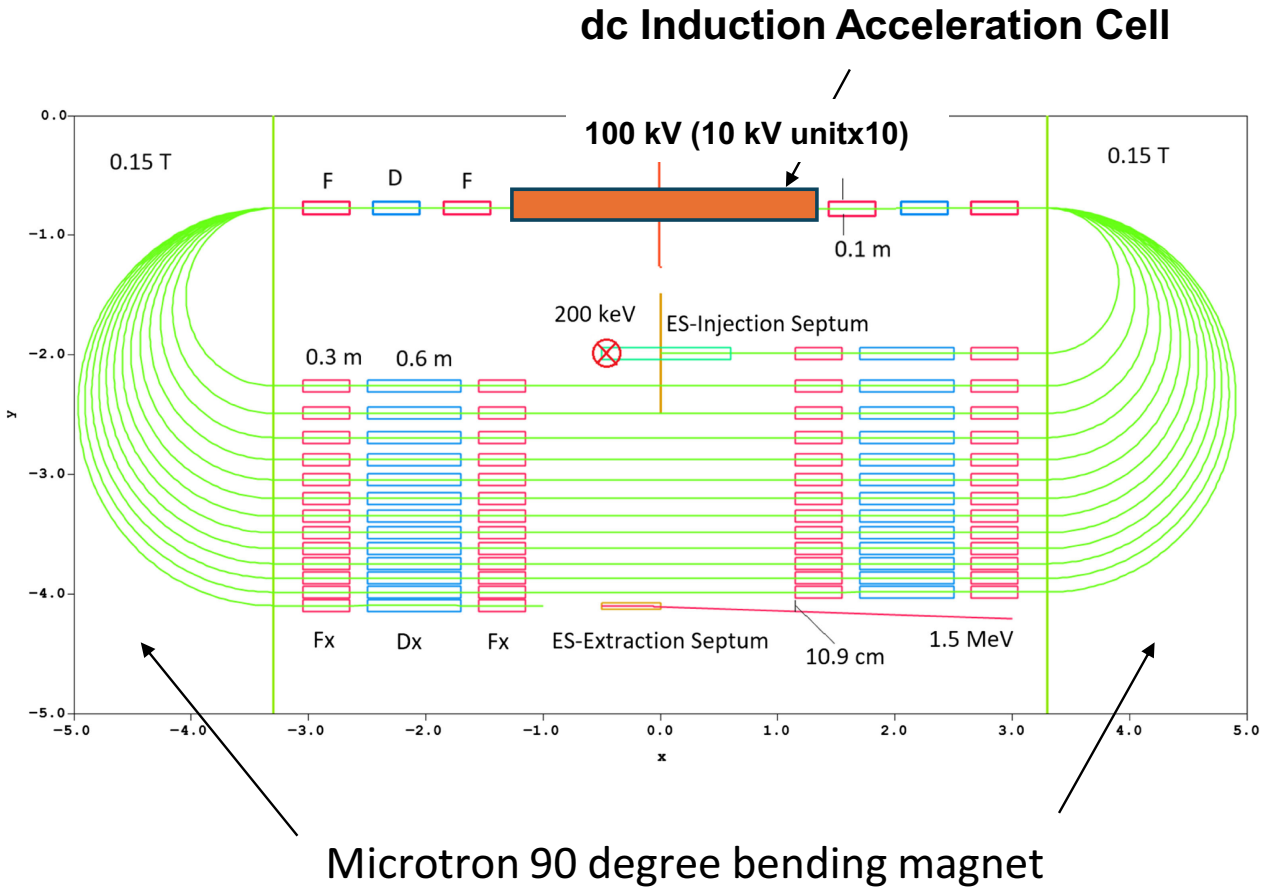

FIG. 11. 1.5 MeV induction microtron.

described by

$$V \cdot \tau = -\Delta B \cdot S,$$

where $S = w \cdot d$ is the cross section of a single disk of magnetic material of thickness d and width w, and ΔB is the magnetic flux swing in the setting of the induction cell. The induction core is provided industrially in the form of a bobbin made of 13-μm-thick nanocrystalline material (Finemet®) tape and with an assumed packing factor of 0.75. Using the bobbin's inner radius r_i and outer radius r_o, w is given by $w = r_o - r_i$. Considering a cell unit with 5 kV dc induction acceleration, and assuming $\tau = 1$ μs, $\Delta B = 0.8$ T, and $d = 2.54 \times 10^{-2}$ m, we obtain $w = 32.8$ cm. Cells A and B, which constitute the dc induction cell unit, have a single induction core bobbin inside their stainless-steel container, which is cooled with pure water or insulating oil. If much higher acceleration voltage is required, then multiple units of this type can be configured in a straight line. The induction acceleration cell for a hadron accelerator such as FFAG with a spiral orbit has no axial symmetry; instead, it is an induction cell with a wide, flat opening shape. If a higher acceleration voltage is required, then much larger induction cells must be designed. In any case, the necessary number of induction cells is placed in the straight sections.

B. dc induction microtron

The idea of an induction microtron (a racetrack-shaped fixed fields induction accelerator) was proposed previously [6] and its beam dynamics have been studied in detail [7]. Hereafter, this is referred to as the original scheme, where 50% duty induction cells are used for acceleration and confinement. The dc induction microtron requires no barrier bucket [3,4], and the 50% duty induction cells in the original scheme are replaced simply with dc induction acceleration cells in the dc scheme. The beam dynamics in the straight section differ notably from those of the original scheme. As shown in Fig. 11, multiple ion beams merge in the straight section; that is, ions injected at different times, which propagate on their own orbits in both bending magnets, merge into a single beam. Ions are exposed periodically to strong space-charge forces. This specific beam-beam effect may limit the allowed beam intensity in the present scheme. This type of accelerator may be attractive as a low-current dc ion accelerator.

C. dc induction FFAG accelerator

Takahashi [5] proposed the idea of an induction FFAG accelerator 23 years ago. As in the dc induction microtron, the 50% duty induction cells must again be replaced by

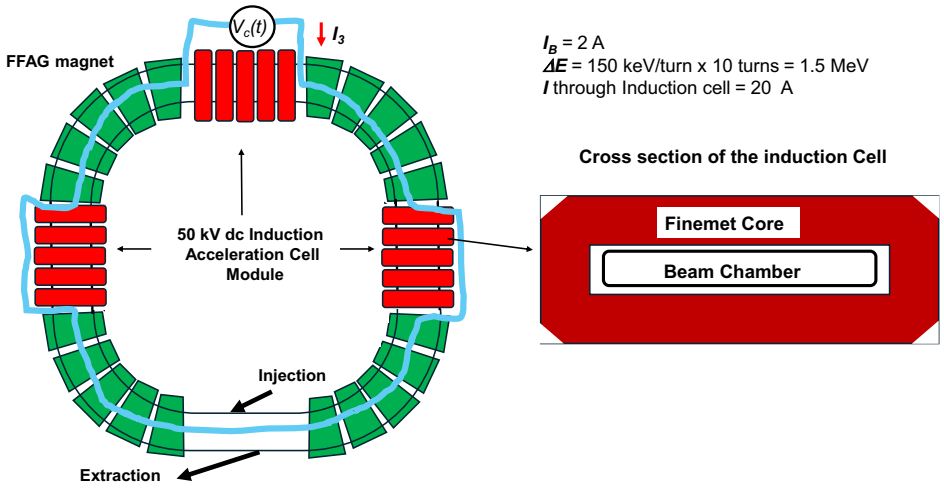

FIG. 12. dc induction FFAG.

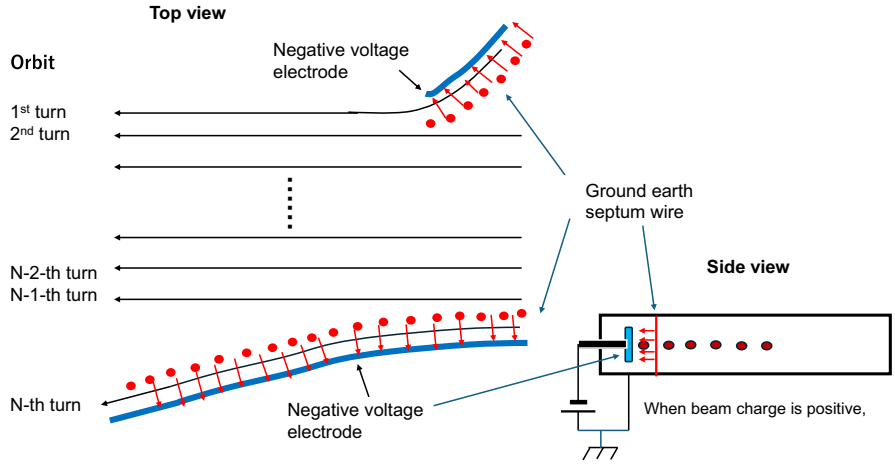

FIG. 13. Injection and extraction method for the dc induction FFAG.

dc induction cells, but with a notably different geometrical shape [14,15], as shown in Fig. 12. The required 10-kV dc induction cell must be horizontally long because of the spiral orbit of the ion beam. Note that the beam current to be accelerated becomes large in proportion to the number of turns; this is an important factor when considering beam loading on the induction cells. The primary loop current I_1 must exceed this beam current, unlike the dc induction microtron, beam separation leads to relaxation of space-charge effects. Figure 12 shows the dc induction FFAG accelerator schematically.

The dc ion beam can be injected and extracted using the high-voltage electrostatic septum shown in Fig. 13, with sufficiently large turn separation preventing the ion beam from hitting the thin wires.

D. Isochronous storage ring with dc acceleration

Takayama [2] argued intensively that a cw FEL can be realized by integrating the isochrony of an electron storage ring and dc induction acceleration. Phase motion freezing in the isochronous storage ring preserves the FEL micro-bunch structure until the next turn, and the FEL micro-bunches start to couple strongly with the seed light from the wiggler entrance, resulting in a large FEL gain. A fraction of the amplified FEL power is divided mechanically and continuously into the seed and the rest, which are returned to the wiggler entrance and guided to the user region using a mirror system. Preliminary computer simulation has demonstrated the feasibility of this [16]. Figure 14 shows the cw EUV-FEL schematically.

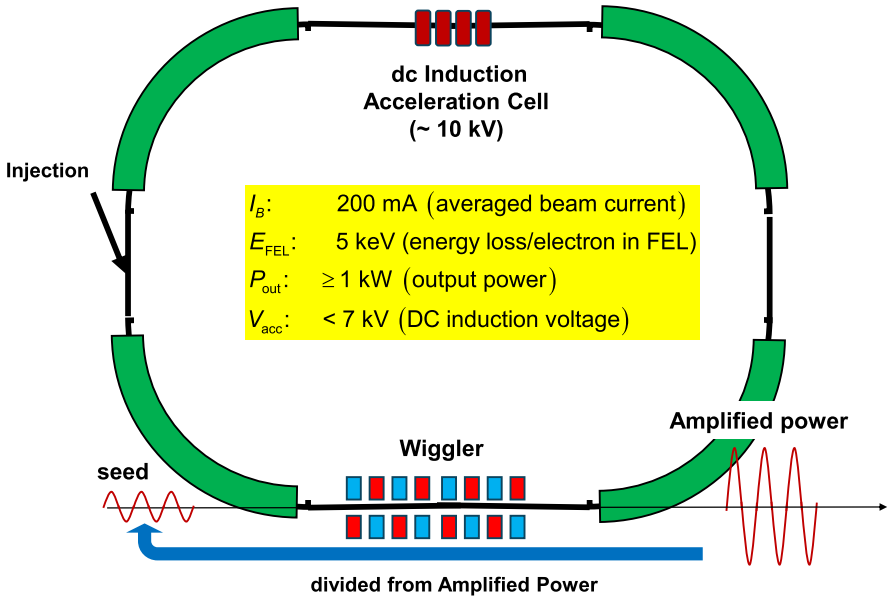

FIG. 14. cw EUV-FEL in a storage ring.

This application does not require a large acceleration voltage, because the role of dc induction acceleration is just to compensate for energy losses, which come from synchrotron radiation and FEL interaction.

VII. SUMMARY

A practical scenario that realizes effective dc acceleration in a circular ring was evaluated in this study. The magnetic cores in the induction acceleration cells must always be reset, and this resetting is done by using diodes to open the electrically closed loop of the outer cage. At this time, the magnetic flux exits the induction acceleration cell, inducing secondary loop current on the metal vacuum chamber. This current accumulates with continuous pulse operation of a pair of induction cells, leading to incomplete resetting of the induction core. To avoid this imperfect resetting, a tertiary current loop coupling with the guiding magnets or an external flux absorber, but not with the induction cores, was introduced; this loop is excited by a compensation voltage power supply so as to cancel the secondary loop current. Consequently, resetting of the induction cores is guaranteed at the expense of excitation of the guiding magnets or the flux absorber. This determines an actual limit on continuous dc induction acceleration, although perturbations of the beam-guiding magnetic fields by the tertiary loop current are negligible during practical beam circulation. These aspects were discussed in detail.

The present concept of secondary loop current compensation requires confirmation given the practical opening/closing characteristics of diodes, and this is under development. The parameters of the compensation voltage profile $V_C(t)$, discussed in Sec. III, depend on the accelerator configuration, especially the beam-guiding magnet system. The first example of the present concept will come from a cw FEL experiment using the NewSUBARU isochronous storage ring [9].

Possible configurations of circular accelerators, which could be very impactful when realized, were also briefly introduced. Most of them are under design by our research team, and details will be released soon. It is expected that unique, interesting, and unknown applications will come from exploring ideas associated with effective dc acceleration.

ACKNOWLEDGMENTS

Professor Weihua Jiang (Nagaoka University of Technology) pointed out the significance of secondary loop current at the early stage of this study. The present authors acknowledge Professor Kazuhiko Horioka (Institute of Science Tokyo), Susumu Takano (KEK), and Akira Tokuchi (PPJ) for stimulated discussions. The present study was financially supported by Grant-In-Aid for Scientific Research (B) (KAKENHI 24K03200).

DATA AVAILABILITY

The data that support the findings of this article are not publicly available upon publication because it is not technically feasible and/or the cost of preparing, depositing, and hosting the data would be prohibitive within the terms of this research project. The data are available from the authors upon reasonable request.

APPENDIX A: CIRCUIT ANALYSIS OF THE PARALLEL CIRCUIT MODEL FOR COMPENSATION

Assumed circuit parameters, including those of the storage ring, are listed in Table I, where the parameters are those of the induction acceleration cell used for the induction synchrotron [3].

Ignoring capacitance, we have for loop 1

$$r \cdot I_1 + V_{\text{cell}} = V, \tag{A1}$$

where

$$Z \cdot i_Z = V_{\text{Cell}} \tag{A2}$$

$$R_1 \cdot i_R = V_{\text{cell}} \tag{A3}$$

$$L_1 \cdot \frac{di_L}{dt} + M_{12} \cdot \frac{dI_2}{dt} = V_{\text{Cell}} \tag{A4}$$

$$I_1 = i_Z + i_R + i_L \tag{A5}$$

with matching condition, $\frac{1}{r} = \frac{1}{Z} + \frac{1}{R_1}$.

From (A1),

$$\begin{aligned} V_{\text{cell}} &= V - r \cdot I_1 \\ \dot{V}_{\text{cell}} &= -r \cdot \dot{I}_1 \end{aligned}. \tag{A6}$$

Using (A2) and (A3), we have

$$i_L = I_1 - i_Z - i_R = I_1 - V_{\text{cell}} \cdot \left(\frac{1}{Z} + \frac{1}{R_1}\right) = I_1 - \frac{V_{\text{cell}}}{r}. \tag{A7}$$

Substituting (A7) into (A4), we have $L_1 \cdot (\dot{I}_1 - \frac{\dot{V}_{\text{cell}}}{r}) + M_{12} \cdot \dot{I}_2 = V_{\text{Cell}}$. Further, substituting (A6) into the above equation, we have $L_1 \cdot (\dot{I}_1 + \dot{I}_1) + M_{12} \cdot \dot{I}_2 = V - r \cdot I_1$.

Using $M_{12} = L_1$

$$2L_1 \cdot \dot{I}_1 + L_1 \cdot \dot{I}_2 + r \cdot I_1 = V. \tag{A8}$$

For loop 2

$$L_1 \cdot \frac{dI_2}{dt} + M_{12} \cdot \frac{dI_1}{dt} + n \cdot V_M + L_3 \cdot \frac{dI_2}{dt} + R_3 \cdot I_2 = 0, \tag{A9}$$

where

$$L_2 \cdot \frac{dI_2^{ML}}{dt} + M_{23} \cdot \frac{dI_3}{dt} = V_M \tag{A10}$$

$$R_2 \cdot I_2^{MR} = V_M \tag{A11}$$

$$I_2 = I_2^{ML} + I_2^{MR} \tag{A12}$$

From (A11) and (A12), we have

$$I_2^{ML} = I_2 - \frac{V_M}{R_2}. \tag{A13}$$

Substitution of (A13) into (A10) yields

$$L_2 \cdot \dot{I}_2 - \frac{L_2}{R_2} \cdot \dot{V}_M + M_{23} \cdot \dot{I}_3 = V_M. \tag{A14}$$

From (A9), $L_1 \cdot \dot{I}_2 + M_{12} \cdot \dot{I}_1 + n \cdot V_M + L_3 \cdot \dot{I}_2 + R_3 \cdot I_2 = 0$ and $M_{12} = L_1$, we have

$$n \cdot V_M = -[(L_1 + L_3) \cdot \dot{I}_2 + L_1 \cdot \dot{I}_1 + R_3 \cdot I_2] \tag{A15}$$

$$n \cdot \dot{V}_M = -[(L_1 + L_3) \cdot \ddot{I}_2 + L_1 \cdot \ddot{I}_1 + R_3 \cdot \dot{I}_2]. \tag{A16}$$

Substituting (A15) and (A16) into (A14), we obtain

$$\begin{aligned} nL_2 \cdot \dot{I}_2 + \frac{L_2}{R_2} \cdot [(L_1 + L_3) \cdot \ddot{I}_2 + L_1 \cdot \ddot{I}_1 + R_3 \cdot \dot{I}_2] \\ + n \cdot M_{23} \cdot \dot{I}_3 = -[(L_1 + L_3) \cdot \dot{I}_2 + L_1 \cdot \dot{I}_1 + R_3 \cdot I_2]. \end{aligned}$$

TABLE I. Circuit parameters of the induction acceleration cell and the typical guiding magnet.

Parameter		L (H)	C (F)	R (Ω)
	Transmission line			$r = 125$
	Matching resistance $1/r = 1/Z + 1/R_1$			$Z = 210$
1	Induction cell	$L_1 = 110\ \mu$	260 P	$R_1 = 330$
2	Typical guiding magnet	$L_2 = \sim 10 \times L_1$		$R_2 = \sim 10 \times R_1$
	Total number of magnets	$N = \sim 50$		
3	Beam chamber	$L_3 = 431\ \mu$	3×10^{-7}	$R_3 = 0.236$

Using $M_{23} = L_2$, we have

$$\frac{L_2}{R_2}\cdot[(L_1+L_3)\cdot\ddot{I}_2 + L_1\cdot\ddot{I}_1] + \left(L_1 + nL_2 + L_2\cdot\frac{R_3}{R_2} + L_3\right)\cdot\dot{I}_2 + L_1\cdot\dot{I}_1 + n\cdot L_2\cdot\dot{I}_3 + R_3\cdot I_2 = 0. \quad \text{(A17)}$$

For loop 3,

$$n\cdot\left(L_2\cdot\frac{dI_3}{dt} + M_{23}\cdot\frac{dI_2^{ML}}{dt}\right) + L_4\cdot\frac{dI_3}{dt} + R_4\cdot I_3 = V_C(t) \Rightarrow n\cdot L_2\cdot\dot{I}_3 + n\cdot L_2\cdot\left(\dot{I}_2 - \frac{\dot{V}_M}{R_2}\right) + L_4\cdot\dot{I}_3 + R_4\cdot I_3 = V_C(t). \quad \text{(A18)}$$

Using (A16) and (A18) reduces to

$$n\cdot L_2\cdot\dot{I}_3 + n\cdot L_2\cdot\dot{I}_2 + \frac{L_2}{R_2}\cdot[(L_1+L_3)\cdot\ddot{I}_2 + L_1\cdot\ddot{I}_1 + R_3\cdot\dot{I}_2] + L_4\cdot\dot{I}_3 + R_4\cdot I_3 = V_C(t)$$

$$[n\cdot L_2\cdot\dot{I}_3 + L_4\cdot\dot{I}_3 + R_4\cdot I_3] + \left\{\frac{L_2\cdot(L_1+L_3)}{R_2}\cdot\ddot{I}_2 + L_2\cdot\left(n + \frac{R_3}{R_2}\right)\cdot\dot{I}_2\right\} + \frac{L_1\cdot L_2}{R_2}\cdot\ddot{I}_1 = V_C(t), \quad \text{(A19)}$$

with initial and boundary conditions

$$I_1(k\cdot\tau) = \dot{I}_1(k\cdot\tau) = 0 \text{ for } k = 0, 1, 2, 3, \ldots, N,$$
$$I_2(0) = \dot{I}_2(0) = 0,$$
$$I_3(0) = \dot{I}_3(0) = 0,$$

where is the switching number and is the time period of reset.

Through τ, $I_2(t)$ must be 0. We have to look for the compensation voltage $V_C(t)$ so as to meet this constraint.

Solution to satisfy $I_2 = 0$

$$2L_1\cdot\dot{I}_1 + r\cdot I_1 = V \quad \text{(A20)}$$

$$\frac{L_1\cdot L_2}{R_2}\cdot\ddot{I}_1 + L_1\cdot\dot{I}_1 + n\cdot L_2\cdot\dot{I}_3 = 0 \quad \text{(A21)}$$

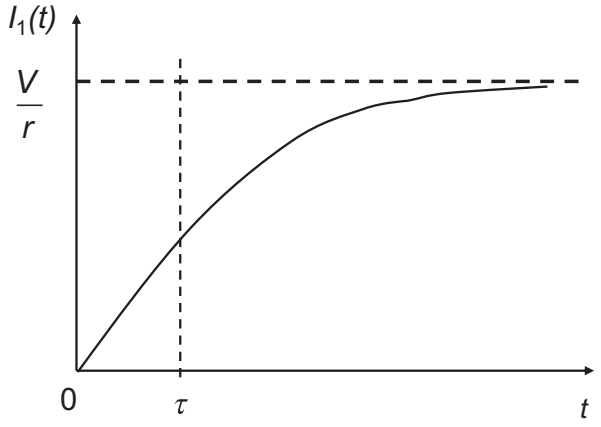

FIG. 15. First loop current $I_1(t)$.

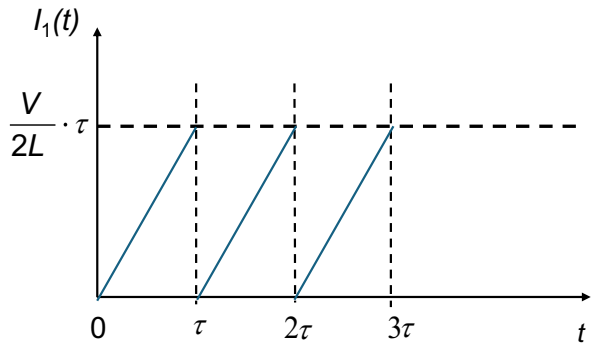

FIG. 16. $I_1(t)$ in the cw operation following (A26).

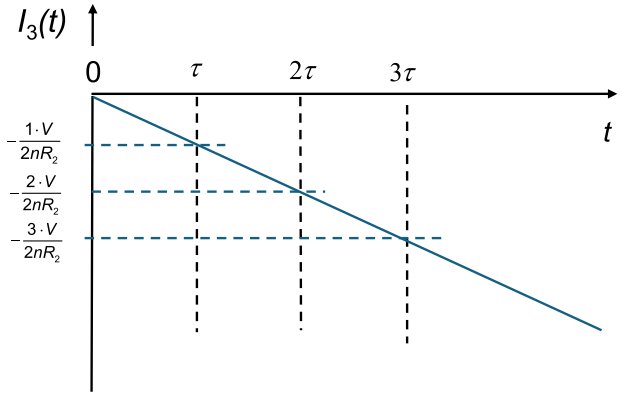

FIG. 17. Third loop current in the cw operation following (A27).

$$n \cdot L_2 \cdot \dot{I}_3 + L_4 \cdot \dot{I}_3 + R_4 \cdot I_3 + \frac{L_1 \cdot L_2}{R_2} \cdot \ddot{I}_1 = V_C(t) \tag{A22}$$

for $k \cdot \tau \le t < (k+1) \cdot \tau$

$$2L_1 \cdot \dot{I}_1 + r \cdot I_1 = V \tag{A23}$$

$$\frac{L_1 \cdot L_2}{R_2} \cdot \dot{I}_1 + L_1 \cdot I_1 + n \cdot L_2 \cdot I_3 = n \cdot L_2 \cdot I_3(k \cdot \tau) \tag{A24}$$

$$L_4 \cdot \dot{I}_3 + R_4 \cdot I_3 - L_1 \cdot \dot{I}_1 = V_C(t) \tag{A25}$$

$I_3(t)$ is obtained from (A23) and (A24). Substituting this $I_3(t)$ into (A25), at last, we have $V_C(t)$.

Solution of (A23) is easily obtained for $k \cdot \tau \le t < (k+1) \cdot \tau$,

$$I_1(t) = \frac{V}{r} \cdot (1 - e^{-r/2L_1 \cdot t}).$$

In the region of $k \cdot \tau \le t < (k+1) \cdot \tau$, it is approximated to

$$I_1(t) \simeq \frac{V}{r} \cdot \frac{r}{2L_1} \cdot (t - k \cdot \tau) = \kappa \cdot (t - k \cdot \tau) \quad \text{with } \kappa = \frac{V}{2L_1}. \tag{A26}$$

Substituting (A26) into (A24), we have

$$\begin{aligned} I_3(t) &= I_3(k \cdot \tau) - \frac{1}{nL_2} \cdot \left(\frac{L_1 \cdot L_2}{R_2} \cdot \dot{I}_1 + L_1 \cdot I_1 \right) = I_3(k \cdot \tau) - \frac{1}{nL_2} \cdot \left[\frac{L_1 \cdot L_2}{R_2} \cdot \kappa + L_1 \cdot \kappa \cdot (t - k \cdot \tau) \right] \\ &= I_3(k \cdot \tau) - \frac{L_1 \cdot \kappa}{nL_2} \cdot \left(\frac{L_2}{R_2} + t - k \cdot \tau \right) = I_3(k \cdot \tau) - \frac{V}{2nL_2} \cdot \left(\frac{L_2}{R_2} + t - k \cdot \tau \right). \end{aligned} \tag{A27}$$

Because of $L_2/R_2 \gg \tau$,

$$I_3[(k+1) \cdot \tau] = I_3(k \cdot \tau) - \frac{V}{2nL_2} \cdot \left(\frac{L_2}{R_2} + \tau \right) \simeq I_3(k \cdot \tau) - \frac{V}{2nR_2}. \tag{A28}$$

It is notified that $\frac{V}{2nR_2} \simeq \frac{2000}{2 \times 50 \times 10 \times 330} A = 3 \times 10^{-3} A$.

Using (A27), (A25) reduces to

$$\begin{aligned} V_C(t) &= -\frac{L_4}{2nL_2} \cdot V + R_4 \cdot I_3(k \cdot \tau) - \frac{R_4 \cdot V}{2nL_2} \cdot \left(\frac{L_2}{R_2} + t - k \cdot \tau \right) - \frac{V}{2} \\ &= R_4 \cdot I_3(k \cdot \tau) - \frac{V}{2} \cdot \left[1 + \left(\frac{L_4}{nL_2} \right) + \left(\frac{R_4}{nR_2} \right) + \left(\frac{R_4}{nL_2} \right) \cdot (t - k \cdot \tau) \right] \\ &= R_4 \cdot I_3(k \cdot \tau) - \frac{V}{2} \cdot \left[1 + \frac{1}{n} \cdot \left(\frac{L_4}{L_2} + \frac{R_4}{R_2} \right) + \left(\frac{R_4}{nL_2} \right) \cdot (t - k \cdot \tau) \right]. \end{aligned} \tag{A29}$$

Considering $L_4 \ll L_2$, $R_4 \ll R_2$, and $n \gg 1$, we arrive at

$$V_C(t) = R_4 \cdot I_3(k \cdot \tau) - \frac{V}{2} \cdot \left[1 + \left(\frac{R_4}{nL_2} \right) \cdot (t - k \cdot \tau) \right] \quad V_C[(k+1) \cdot \tau] = R_4 \cdot I_3(k \cdot \tau) - \frac{V}{2} \cdot \left[1 + \left(\frac{R_4}{nL_2} \right) \cdot \tau \right]. \tag{A30}$$

Because of $(\frac{R_4}{nL_2}) \cdot \tau \ll 1$,

$$V_C((k+1) \cdot \tau) \simeq R_4 \cdot I_3(k \cdot \tau) - \frac{V}{2}. \tag{A31}$$

From (A31), it is clear that the compensation voltage V_C must increase linearly with an offset of $V/2$. When R_4 and L_4 in the third loop are of the same order as those of the second loop, I_3 reaches 3 A after 10^3 resets, which means that $V_C(10^3\tau) \sim V/2$. Roughly speaking, the compensation voltage of about 1 kV seems to be required when $V = 2$ kV.

APPENDIX B: COMPARISON WITH A VERY LARGE-SCALE INDUCTION CELL

Introduction of the magnetic flux storage into the present dc induction acceleration system may be conceptually regarded as induction acceleration employing a very large induction acceleration system with a single acceleration gap nearby the magnetic core [17], in that it is operated in a trivial way, but the induced voltage pulse length is generated much longer than the revolution time period in a circular accelerator of interest. This long-pulse induction acceleration method was considered at the early stage of FFAG accelerator development [18,19], in which the induced voltage associated with the rising of the guiding magnetic flux was employed for acceleration for many turns at the early stage of acceleration, and then an rf voltage was adopted to take over the role up to a final energy.

Here a millisecond-order-long pulse is considered, by which continuous acceleration is enabled for more than 2000 turns in an electron storage ring of 120 m in circumference [8]. These 2000 turns are regarded as a kind of guideline of beam refreshing rate forced due to beam quality degradation. Meanwhile, a total circulating time period from injection to extraction in hadron accelerators of current interest, such as FFAG accelerator or microtron, may be around 100 μs. Continuous operation is, in principle, carried out with a duty factor of 50%; resetting of the magnetic flux is required during the next 1 ms.

The millisecond-long-pulse induction acceleration cell is required to have a large cross section of the magnetic core, similar to that of the magnetic flux storage described in this study. Its inductance is required to be extremely large, and core loss is generally regarded as being proportional to inductance. The droop voltage, which is expressed by

$$V(t) \simeq V_0 \cdot \exp[-R/(2 \cdot L) \cdot t],$$

where R is the core loss and L is the inductance, simply decreases in proportion to the pulse length. Beyond 1 ms, the voltage decrease due to droop is significant in a nominal induction core [20]. In order to reduce the droop, it is effective to increase L while avoiding an increase of R. The simplest method is to wind the primary wiring in multiple layers [21]. However, it necessarily involves a reduction of the induced voltage. To date, droop compensation methods have been proposed. A technique has been suggested in which several pulse voltages of half sine in time are superimposed, and this may be effective in a realistic manner [22]. Multiple induction modules are stacked in an additional single induction unit. Each induction module is driven independently by its own pulse modulator. Each pulse modulator is triggered in some programmed manner with a desired voltage so that the superimposed voltage at the induction gap is provided with the required flat profile. However, this system is too complicated and costly for the present use.

The problem of this droop appears in a different form in the magnetic flux storage scheme scenario. As shown in Eq. (A30) or (A31), the compensation voltage must be managed in time for the time period of continuous operation in order to maintain $I_2 = 0$. This is not regarded as a big issue, but it is left as a topic for discussion elsewhere.

[1] K. Takayama, Japan Patent No. 7483285 (2024).
[2] K. Takayama, Effective dc acceleration in a circular accelerator and its application, Sci. Rep. **13**, 13595 (2023).
[3] *Induction Accelerators*, edited by K. Takayama and R. J. Briggs (Springer-Verlag, Berlin, Heidelberg, 2011), Chap. 11.
[4] K. Takayama, Evolution of induction synchrotrons, Rev. Phys. **10**, 100083 (2023).
[5] H. Takahashi, Super-bunch acceleration scheme in FFAG, in *Proceedings of RPIA2002: The International Workshop on Recent Progress in Induction Accelerators, Tsukuba* (2002), p. 33.
[6] K. Takayama, T. Adachi, M. Wake, and K. Okamura, Racetrack-shape fixed field induction accelerator for giant cluster ions, Phys. Rev. ST Accel. Beams **18**, 050101 (2015).
[7] Taufik, T. Adachi, M. Wake, and K. Takayama, Beam dynamics of the racetrack-shape fixed field induction accelerators, Phys. Rev. ST Accel. Beams **22**, 044001 (2019).
[8] A. Ando, S. Amano, S. Hashimoto, H. Kinoshita, S. Miyamoto, T. Mochizuki, M. Niibe, Y. Shoji, M. Terasawa, T. Watanabe, and N. Kumagai, Isochronous storage ring of the new SUBARU project, J. Synchrotron Radiat. **5**, 342 (1998).
[9] S. Hashimoto (private communication).
[10] COMSOL Multiphysics software, https://www.comsol.jp.
[11] M. Q. Tran *et al.*, Status and future development of heating and current drive for the EU DEMO, Fusion Eng. Des. **180**, 113159 (2022).
[12] Y. Liu, K. Okamura, and K. Takayama, Fourth generation switching power supply for circular induction accelerators, Rev. Sci. Instrum. **94**, 053304 (2023).
[13] *Induction Accelerators*, edited by K. Takayama and R. J. Briggs (Springer, Berlin, 2011), Chaps. 5 and 11.
[14] K. Takayama, T. Adachi, and J. Hasegawa, Japan Patent PAT01589 (2026).
[15] K. Takayama, T. Adachi, K. Egawa, K. Okamura, and J. Hasegawa, DC induction FFAG (to be published).
[16] F. Sakamoto (private communications).
[17] K. Imai (private communication).

[18] K. M. Terwilliger, L. W. Jones, D. W. Kerst, and K. R. Symon, Application of FFAG principle tobetatron acceleration, Report No. MURA-041, MURA, 1953.

[19] L. W. Jones and K. M. Terwilliger, A MARK Ib betatron design, Report No. MURA-053, MURA, 1955.

[20] Y. Shimosaki, E. Nakamura, K. Takayama, K. Torikai, M. Watanabe, M. Nakajima, and K. Horioka, Beam-dynamic effects of a droop in an induction accelerating voltage, Phys. Rev. ST Accel. Beams **7**, 014201 (2004).

[21] T. Iwashita, T. Adachi, K. Takayama *et al.*, KEK digital accelerator, Phys. Rev. ST Accel. Beams **14**, 071301 (2011).

[22] K. Horioka, M. Nakajima, M. Watanabe, M. Honda, E. Hotta, M. Shiho, M. Ogawa, J. Hasegawa, J. Kishiro, and K. Takayama, Repetitive induction voltage modulator for heavy ion fusion, Laser Part. Beams **20**, 609 (2002).